Published online 27 September 2022 *Nucleic Acids Research, 2022, Vol. 50, No. 18* **10601–10613**
https://doi.org/10.1093/nar/gkac837

Nanopore tweezers measurements of RecQ conformational changes reveal the energy landscape of helicase motion

Jonathan M. Craig [1,*], Maria Mills[2,3], Hwanhee C. Kim[1], Jesse R. Huang[1], Sarah J. Abell[1], Jonathan W. Mount[1], Jens H. Gundlach[1], Keir C. Neuman[2] and Andrew H. Laszlo [1]

[1]Department of Physics, University of Washington, 3910 15th Ave NE, Seattle, WA, USA, [2]Laboratory of Single Molecule Biophysics, National Heart, Lung, and Blood Institute, National Institutes of Health, Bethesda, MD 20892, USA and [3]Department of Physics & Astronomy, University of Missouri, 701 S College Ave, Physics Building Rm 223, Columbia, MO 65211, USA

Received February 16, 2022; Revised September 02, 2022; Editorial Decision September 12, 2022; Accepted September 19, 2022

ABSTRACT

Helicases are essential for nearly all nucleic acid processes across the tree of life, yet detailed understanding of how they couple ATP hydrolysis to translocation and unwinding remains incomplete because their small (∼300 picometer), fast (∼1 ms) steps are difficult to resolve. Here, we use Nanopore Tweezers to observe single *Escherichia coli* RecQ helicases as they translocate on and unwind DNA at ultrahigh spatiotemporal resolution. Nanopore Tweezers simultaneously resolve individual steps of RecQ along the DNA and conformational changes of the helicase associated with stepping. Our data reveal the mechanochemical coupling between physical domain motions and chemical reactions that together produce directed motion of the helicase along DNA. Nanopore Tweezers measurements are performed under either assisting or opposing force applied directly on RecQ, shedding light on how RecQ responds to such forces *in vivo*. Determining the rates of translocation and physical conformational changes under a wide range of assisting and opposing forces reveals the underlying dynamic energy landscape that drives RecQ motion. We show that RecQ has a highly asymmetric energy landscape that enables RecQ to maintain velocity when encountering molecular roadblocks such as bound proteins and DNA secondary structures. This energy landscape also provides a mechanistic basis making RecQ an 'active helicase,' capable of unwinding dsDNA as fast as it translocates on ssDNA. Such an energy landscape may be a general strategy for molecular motors to maintain consistent velocity despite opposing loads or roadblocks.

INTRODUCTION

Helicases are molecular machines that hydrolyze ATP to unwind or remodel nucleic acids. They are involved in all aspects of genome maintenance, from replication and transcription to damage repair and removal of bound proteins (1–4). Helicases can be broadly divided into six superfamilies, the largest of which is superfamily 2 (SF2). SF2 helicases have conserved structural features, but exhibit a broad range of activities (5). SF2 helicases share a common core motor composed of two RecA-like domains, which couple ATP binding and hydrolysis to translocation along DNA or RNA in single-nucleotide steps in an inchworm-like fashion (6–8). Understanding the general dynamical features of SF2 translocase activity and the details that lead to different behaviors among SF2 helicases is challenging due to the small scale of the domain motions and the velocity at which they move (10s to 1000s of nucleotides/second).

The highly conserved family of RecQ helicases is a subgroup of SF2 helicases that are essential for genome integrity. In humans, mutations in RecQ helicases are associated with several disorders characterized by premature aging and a predisposition to cancer (9). RecQ helicases unwind double-stranded DNA (dsDNA) by translocating 3′ to 5′ on one strand while displacing the other strand (3,9–16) and can unwind complex secondary structures in DNA such as G-quadruplexes (17–20).

Single-molecule experiments have revealed molecular details of how RecQ helicases use the energy of ATP hydrolysis to generate mechanical work (21–24). However, resolving individual steps of RecQ is beyond the spatial and temporal resolution of most single-molecule approaches. Here, we leverage the spatiotemporal resolution

*To whom correspondence should be addressed. Tel: +1 206 685 2428; Fax: +1 206 685 0635; Email: jomcraig@uw.edu

of Single-molecule Picometer Resolution Nanopore Tweezers (SPRNT, Nanopore Tweezers) to characterize the kinetics and mechanochemistry of *Escherichia coli* RecQ helicase at previously unresolved detail (25–27). These experiments enable us to identify both common features of SF2 helicase activity and those unique to RecQ.

In SPRNT, a single protein nanopore derived from Mycobacterium smegmatis porin A (MspA) embedded in a phospholipid bilayer is used to monitor the progression of a motor enzyme moving on DNA (Figure 1A–C, materials and methods, Supplementary Figure S1, Supplementary Table S1 and S2). The bilayer divides a salt solution into two wells, called *cis* and *trans*, and a voltage applied across the bilayer establishes an electric field within the pore constriction that causes an ion current to flow through the pore. The ion current is the primary observable in SPRNT experiments. Negatively charged DNA bound to a motor enzyme within the *cis* well is drawn through the pore by the electric field until the enzyme comes to rest on the rim of the pore. The force on the DNA is proportional to the voltage applied across the bilayer (∼0.2 pN/mV). The ion current changes in response to the DNA bases in the narrowest section of the pore ('the constriction'). Enzymatic activity by RecQ then causes motion of the DNA through the pore, and different ion currents are measured as different DNA bases pass through the pore constriction (Figure 1D and E). This provides a record of the DNA sequence passing through the pore. If the DNA sequence is known, this signal reveals the location of the motor enzyme along the DNA strand.

Figure 1E shows the SPRNT (ion current) signal associated with progression of a DNA moved through MspA by RecQ, illustrating how the DNA sequence is identified by the pattern of ion current states. The ion current is then converted to the nucleotide position of the motor enzyme by a non-linear transformation function (Figure 1F) (25,26). In this data, the step dwell time (time spent at a single sequence position) and frequency of backwards steps are key observables that shed light on the underlying enzyme kinetics. Because an enzyme's position is measured by identifying the underlying nucleic acid sequence, the enzyme kinetics can be associated with the underlying DNA sequence revealing sequence-dependent effects (27–30).

In contrast to other force-based techniques such as optical or magnetic tweezers, which typically affect motor motion indirectly by destabilizing the DNA duplex, in SPRNT an assisting or hindering force is applied directly to the enzyme as it moves along the DNA. Depending on whether the 3′ or 5′ end is threaded through the pore, the force applied by the electric field either assists or opposes the predominant motion of the motor enzyme. By testing a motor enzyme in both geometries, nanopore tweezers can probe the effect of opposing and assisting forces on activity (Figure 1A–C). Application of an opposing force directly on the helicase closely mimics physiologically important collisions between the translocating helicase and proteins bound to, or secondary structures such as G-quadraplexes formed in, the nucleic acid substrate. Furthermore, some motor enzymes rest on the pore in a manner such that conformational changes of the motor enzyme result in DNA motion through the pore, enabling detection of kinetic substates (27). For example, in SPRNT measurements of the SF2 helicase Hel308, two distinct kinetic sub-steps were observed per nucleotide translocated (25,27). One sub-step was ATP-concentration-dependent ([ATP]-dependent) whereas the second was ATP-concentration-independent ([ATP]-independent), corresponding to open and closed conformations of the Hel308 RecA-like domains, respectively.

Here, we perform SPRNT measurements of *E. coli* RecQ. We directly observe and quantify the coupling between the ATP hydrolysis cycle and RecQ domain motion, and we use force spectroscopy to map the energetic landscape of RecQ translocation. These results extend and generalize previous results obtained with Hel308 and allow us to determine the common translocation mechanism employed by SF2 helicases. Kinetic analysis of SPRNT data reveals how RecQ couples ATP binding and hydrolysis to internal domain motions that power DNA translocation and unwinding. Furthermore, measuring force-dependent changes in the kinetics of multiple sub-steps in the RecQ catalytic cycle provides a high-resolution energetic landscape of the helicase proceeding through its coupled ATP hydrolysis and translocation pathways.

MATERIALS AND METHODS

A single M2-NNN MspA nanopore was established in a 1,2-di-*O*-phytanyl-*sn*-glycero-3-phosphocholine (DOPHPC, Avanti Polar Lipids) lipid bilayer using methods that have been well established (26).

All experiments were run at room temperature 22 ± 1°C and pH 8.0 buffered with 10 mM HEPES; the *trans* well contained 500 mM KCl while the *cis* well contained 100 mM KCl and 10 mM $MgCl_2$. Pores were established in symmetric salt conditions with 500 mM KCl in both *cis* and *trans* wells and once a single M2-NNN MspA nanopore was established, a buffer with the above conditions along with ATP, ADP and/or ATPγS was perfused to the *cis* well. DNA, DTT and RecQ were added to final concentrations of 10, 1 and 50 nM, respectively. The perfusion was repeated periodically, every 45 min, to maintain constant concentrations of the reactants/products in the reaction volume.

M2-NNN mutant MspA (accession number CAB56052.1) was prepared as described previously, and is identical to WT MspA with the exception of six mutations: D90N, D91N, D93N, D188R, D134R, E193K (26,31). We used a RecQ mutant lacking the Helicase-and-RNaseD-C-terminal (HRDC), which was prepared as described in (22). The structure shown in Figure 1D is from *C. sakazakii* (PDB accession 6CRM, (17)).

Data was acquired with custom labview software on an Axopatch 200B amplifier at 50 kHz sampling frequency, and downsampled by averaging to 25 kHz or 10 kHz. For visualization, ion-current vs. time traces were converted to position vs. time traces as described in (25–27), however in-depth kinetic analysis was performed on ion-current data. Ion current patterns were compiled into a consensus sequence (Supplementary Figure S1 and discussion) and compared to predictions based on the DNA sequence for an enzyme moving in 1-step-per-nucleotide and 2-steps-per-nucleotide. Reads could be confidently identified with the 2-step prediction. At saturating [ATP] nanopore reads

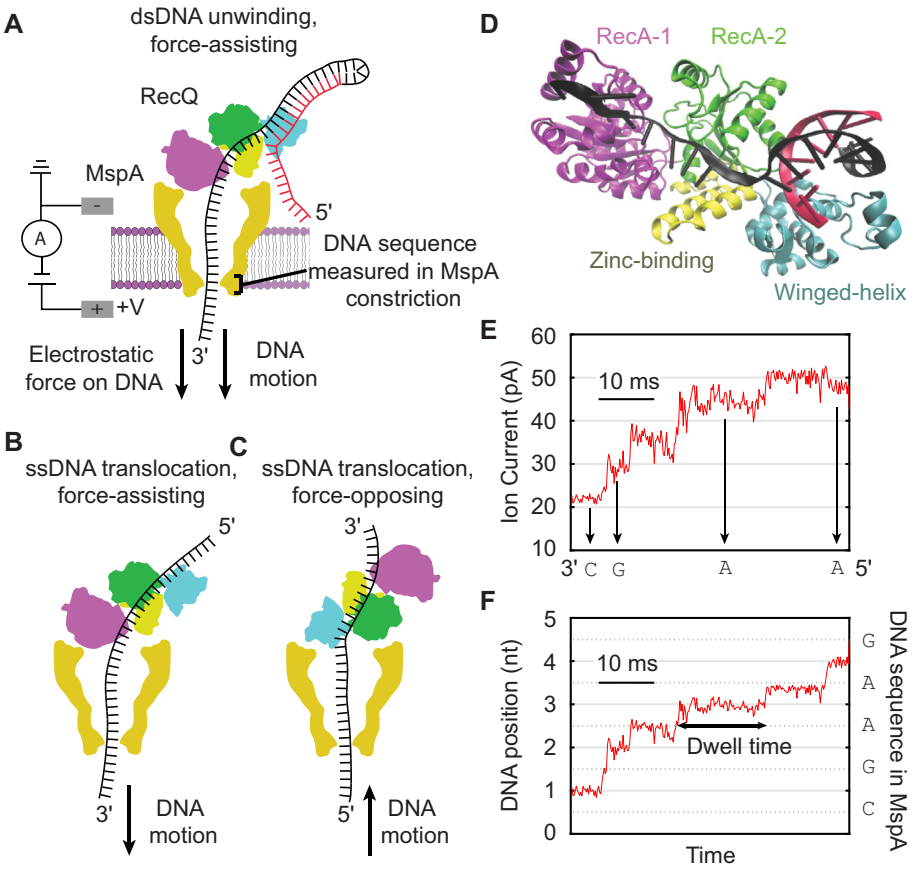

Figure 1. SPRNT measurements of RecQ helicase. (**A**) A single RecQ unwinding dsDNA is drawn into the MspA pore via the single-stranded 3′ end of the template DNA strand. In this configuration, the electrophoretic force on the DNA is in the direction of the DNA motion, assisting RecQ unwinding. (**B**) RecQ translocation on ssDNA with the 3′ end through the pore (assisting force). (**C**) RecQ translocation on ssDNA with the 5′ end through the pore (opposing force). (**D**) Crystal structure of RecQ from *C. sakazakii* bound to dsDNA (PDB 6CRM, 17). Protein domains are: RecA1 (pink), RecA2 (green), zinc binding (yellow), and Winged helix (blue). (**E**) Ion current versus time. The DNA sequence is identified by measuring the pattern of ion current states. (**F**) DNA position vs. time trace of the data shown in (E). Sub-nucleotide steps of the DNA through MspA (dashed horizontal lines) are clearly resolvable with sub-millisecond dwell times. The DNA sequence within the nanopore constriction is indicated on the right axis.

lasted several hundred milliseconds and moved DNA ∼10 nt through the pore. Dwell times at each DNA position were determined by aligning ion-current segments to the corresponding ion current consensus as in (27,28). Step size was measured by determining the ion current consensuses for the [ATP]-dependent and [ATP]-independent states as spline curves, and then minimizing the distance between them (25). We find that $x_{\text{step1}} = 0.56 \pm 0.02$ nt for the forward step from the [ATP]-dependent state to the [ATP]-independent state in both assisting and opposing force conformations whereas the distance from the [ATP]-independent state to the [ATP]-dependent state is $x_{\text{step2}} = 0.44$ nt $\pm$ 0.02 nt.

Observable states in single-molecule experiments are typically composed of several chemical or physical substates, such as ATP binding or a conformational change, respectively. Previous work has shown that the observable dwell times depend on the kinetic path leading into and out of an observable state (27,29,32,33). The kinetics of a forwards step that follows a forwards step may differ from a forwards step that follows a backwards step because different kinetic pathways lead to these two different step types (Supplementary Figures S2 and S3). By analyzing how step types respond to experimental conditions ([ATP], [ADP], [ATPγS], direction and magnitude of the external force), we can make inferences about an enzyme's kinetic pathways (SI Appendix). As shorthand to describe these different scenarios, we use the following notation to denote enzyme step types: fIf (forwards step following a forwards step), fIb (forwards step following a backwards step), etc.

Full DNA design concepts are discussed in supplemental section 1.10 (Supplementary Figure S4). DNA strands were suspended in 100 mM KCl at 20 μM concentration. Hairpin DNA sequences were diluted further to 1 μM and annealed by heating to 90°C and cooled rapidly to 4°C. Sequences which required binding to a complement were annealed at 90°C and then decreased step wise by 10°C/min to 4°C. Once annealed these sequences were diluted to 1 μM prior to addition to the experiment.

The structure of RecQdH bound to ATPγS (PDBID 1OYY (34)) was used as a starting structure for simulations of the effect of ATP/ADP binding on RecQ structure. For the apo state, the structure without ATPγS, PDBID 1OYW was used. For the ADP and ATP simulations, it was

replaced with the appropriate nucleotide. The coordinated Mg^{2+} ion was also included. The systems were minimized in vacuum then solvated in a ∼10 nm × 8.5 nm × 7.5 nm box of TIP3P water molecules and Na^+ and Cl^- ions to a salt concentration of 50 nM. A zinc ion was bound to the Zn-binding site of the Zn finger domain. Parameters for the Zn-coordinating cysteines were modified using the methods described in Brendenberg and Nillson (35). The fully solvated systems were minimized and equilibrated at constant temperature and pressure for 500ps with the protein harmonically restrained at $k = 5$ kcal/mol/Å^2. Pressure was held at 1.01325 bar using Berendsen's method. The systems were then equilibrated without restraints for an additional 2 ns using constant volume and temperature. Temperature was maintained at 300 K using a Langevin thermostat. After equilibration, production runs of 50 ns were conducted for each system. All simulations were run in NAMD (36) and results were visualized in VMD (37).

RESULTS

ATPase activity of RecQ unwinding and ADP inhibition

To probe the mechanism of RecQ translocation on DNA, we conducted force-assisted unwinding experiments, recording more than 150 traces of RecQ unwinding short DNA hairpins at saturating [ATP]. Typical unwinding traces were ∼500 ms long, during which ∼10 bases were unwound on average before the RecQ helicase disassociated from the DNA (Supplemental Figure S1). The DNA moved through the MspA pore in two, approximately one-half nucleotide, steps per nucleotide translocated by RecQ. Similar sub-nucleotide-steps (sub steps) were observed in Nanopore Tweezers measurements of Hel308 helicase translocation on ssDNA. These sub steps enable precise determination of the order of chemical reactions that produce physical motion of the helicase (25,27).

To assign these sub-steps to chemical reactions in the helicase catalytic cycle, we varied the ATP and ADP concentrations and observed how the sub-step dwell times were affected (24,28,29). We found that the sub steps at half-integer DNA positions are [ATP]-dependent, whereas the sub-steps at integer DNA positions are [ATP]-independent (Figure 2A). In ADP titration experiments, increasing [ADP] caused the dwell time of the [ATP]-dependent state to increase, but did not change the dwell time of the [ATP]-independent state (Figure 2B). This suggests that ADP binding/unbinding occurs during the [ATP]-dependent state, during which it competes with ATP binding (Figure 2). We then performed a simultaneous titration of ATP and ADP to test this hypothesis. Figure 2C shows the dwell time versus [ATP] for three different ratios of ADP to ATP: [ADP] = 0, [ADP] = [ATP] and [ADP] = 4[ATP]. The data were best fit by a competitive inhibition model. An alternative model in which ATP binding rectifies the helicase motion after translocation is ruled out in supplementary analysis (Discussion S2, Supplementary Figure S5). The dwell time of the [ATP]-independent state is fully independent of both [ATP] and [ADP] across the entire range of experiments (Figure 2D).

These results can be interpreted within the context of the inchworm model of SF2 helicase motion (30,1,8) and structural data that show conformational changes of RecQ upon ATP binding (34). ATP binds RecQ in the [ATP]-dependent (open) state, driving a conformational change in the RecA-like domains from open to closed (Figure 2E). Due to the position of the helicase on the entry of the pore, this conformational change results in a ∼1/2 nucleotide motion of the DNA through the pore. ATP is hydrolyzed in the [ATP]-independent (closed) state, after which the RecA-like domains return to the open conformation resulting in another net ∼1/2 nucleotide motion of DNA through the nanopore. Finally, ADP is released, completing one catalytic cycle, resulting in a net motion of 1 nucleotide through MspA (movie S1). As the RecA-like domains of RecQ cycle between open and closed conformations, coordinated changes in the relative ssDNA-binding-energies of the two domains enable directed motion along the DNA (1). The similarity of these results to those obtained with Hel308, a distantly related SF2 helicase, suggest this may be a universal feature of processive SF2 helicase motion.

Sequence-dependent ATPγS hydrolysis by RecQ

To gain further insight into the mechanism of ATP hydrolysis we used the ATP analogue ATPγS, which induces ∼1 s-long pauses in, and is known to be hydrolysable by, RecQ (24). In unwinding experiments with [ATP] = 1000 μM and [ATPγS] = 500 μM, we observed pauses of ∼50 milliseconds to >1 s (Figure 3A, B, Supplementary Figure S6), with most of the time spent in the [ATP]-independent state (closed conformation). We also often observed frequent backwards steps that were rarely observed in the absence of ATPγS (Figure 3B). The dwell times of the [ATP]-dependent state were unchanged by the addition of ATPγS. However, we observed that the dwell times of the [ATP]-independent state depended on the position of the nucleotide in the pore, suggesting that RecQ kinetics depend on the DNA sequence (Figure 3A–D).

Figure 3C shows the dwell time distributions for four [ATP]-independent states in the presence and absence of ATPγS for both forwards and backwards steps. At nucleotide positions 1 and 4, RecQ exhibited long pauses (∼1 s) with minimal backwards stepping in the [ATP]-independent state (Figure 3C, D), followed by a forward transition to the next [ATP]-dependent state. At nucleotide positions 2 and 3, RecQ exhibited shorter pauses (∼150 ms) in the [ATP]-independent state with frequent transient backwards steps to the previous [ATP]-dependent state, before eventually moving forwards via a short dwell-time state. These final, short dwell-time steps following a pause had similar dwell-times to those observed in the absence of ATPγS, suggesting that the kinetics of the final transition forwards are due to ATP rather than ATPγS at these positions (Figure 3B–D).

These observations lead to a model in which ATPγS binds to RecQ in the [ATP]-dependent state, triggering the conformational change that closes the RecA-like domains in the same manner as ATP (Figure 2E). However, depending on the position of RecQ along the nucleotide sequence, the helicase behaves differently with ATPγS bound. At DNA positions 1 and 4 the closed state most often transitions directly forwards to the next (open) state, imply-

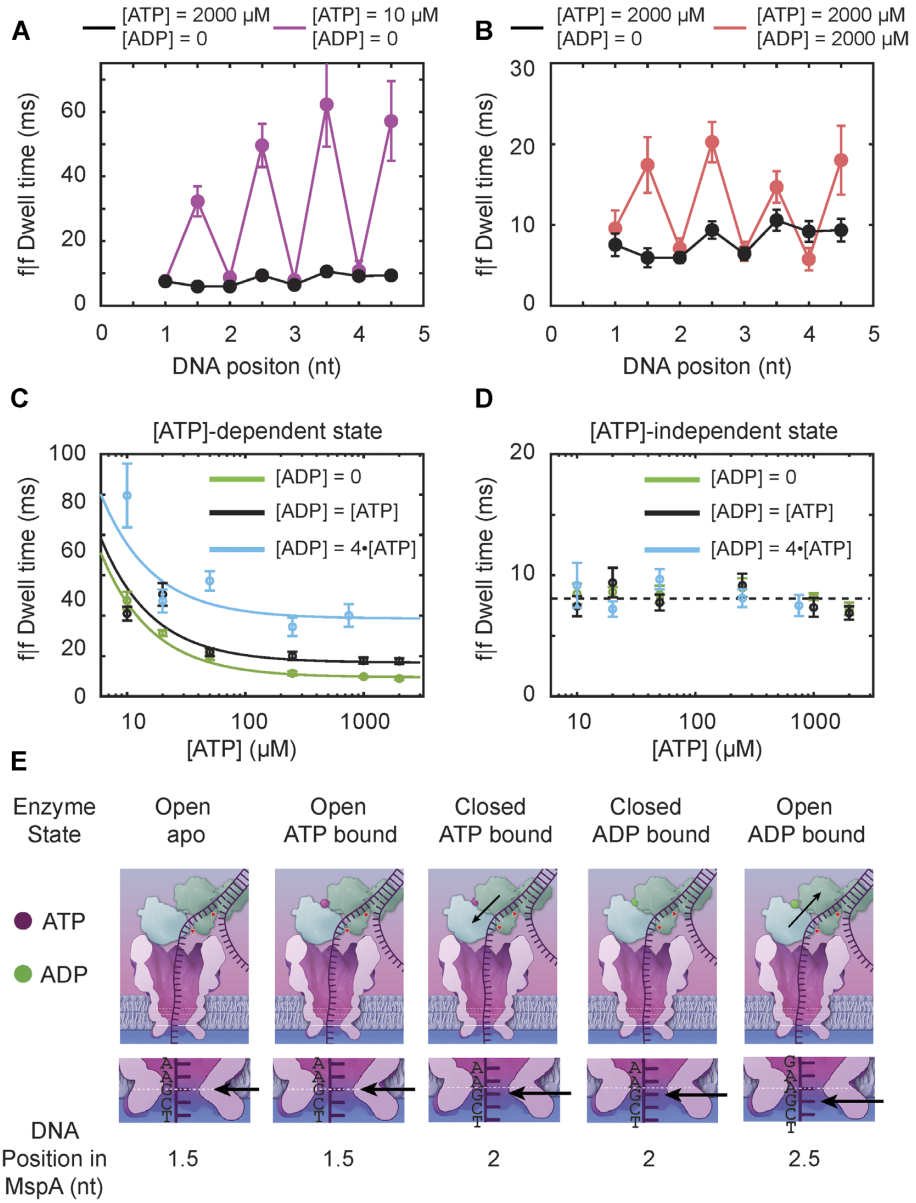

Figure 2. ATP and ADP kinetics of RecQ. (**A**) Dwell-time vs. DNA position for the DNA positions shown in Figure 1E at [ATP] = 2000 μM (black) and [ATP] = 10 μM (pink). (**B**) Dwell-time versus DNA position at [ATP] = 2000 μM with [ADP] = 0 (black) and at [ATP] = 2000 μM with [ADP] = 2000 μM (red). All errors are SEM. (**C**) f|f dwell time of the [ATP]-dependent state (half-integer positions in panel A) versus [ATP] for several ratios of [ADP] to [ATP]: [ADP]/[ATP] = 0 (green), [ADP] = [ATP] (black) and [ADP] = 4 [ATP] (blue). The lines are the fit to a competitive inhibition model (Equation S5, Supporting Information). (**D**) same as left, but for the [ATP]-independent state. (**E**) Model of RecQ unwinding. The helicase starts in the open conformation with no nucleotide bound. ATP and ADP compete for the active site. After ATP binding, the RecA-like domains come together and RecQ shifts on the pore rim resulting in DNA motion of ∼1/2 nt through the pore. ATP is hydrolyzed during the closed state. The RecA-like domains then open, shifting RecQ again on the pore rim moving the DNA through the pore constriction. ADP release completes the ATPase cycle, with a full 1-nt motion along the DNA and one DNA base pair unwound.

ing that RecQ can slowly hydrolyze ATPγS. At DNA positions 2 and 3, RecQ most often transitions from the closed state backwards to the previous open state. The final visit to the closed state at positions 2 and 3 typically has the same dwell time as steps when only ATP is present, implying that ATPγS unbinds from RecQ in the open conformation, enabling ATP to bind before RecQ proceeds through ATP hydrolysis and translocation forward (Figure 3E).

These data are consistent with previous measurements of ATPγS hydrolysis by RecQ: the reported ATPγS hydrolysis rate by RecQ is ∼0.2 s^{-1}, the ATPγS off rate is much faster, and is the primary pause escape pathway (22). Here we measure the ATPγS hydrolysis rate to be 0.5–1 s^{-1} (Discussion S3) but at DNA positions 2 and 3 the likelihood of hydrolyzing ATPγS is very small due to the comparatively large backstepping rate. For example, we find that the opening rate of the helicase at position 2 is more than a factor of 100 larger than at position 1, whereas the ATPγS hydrolysis rate is similar (Discussion S3). Although an insufficient number of DNA sequences were measured to determine the exact sequence dependence of ATPγS hydrolysis, Nanopore Tweezers studies of Hel308 (27,28) and PcrA (30)

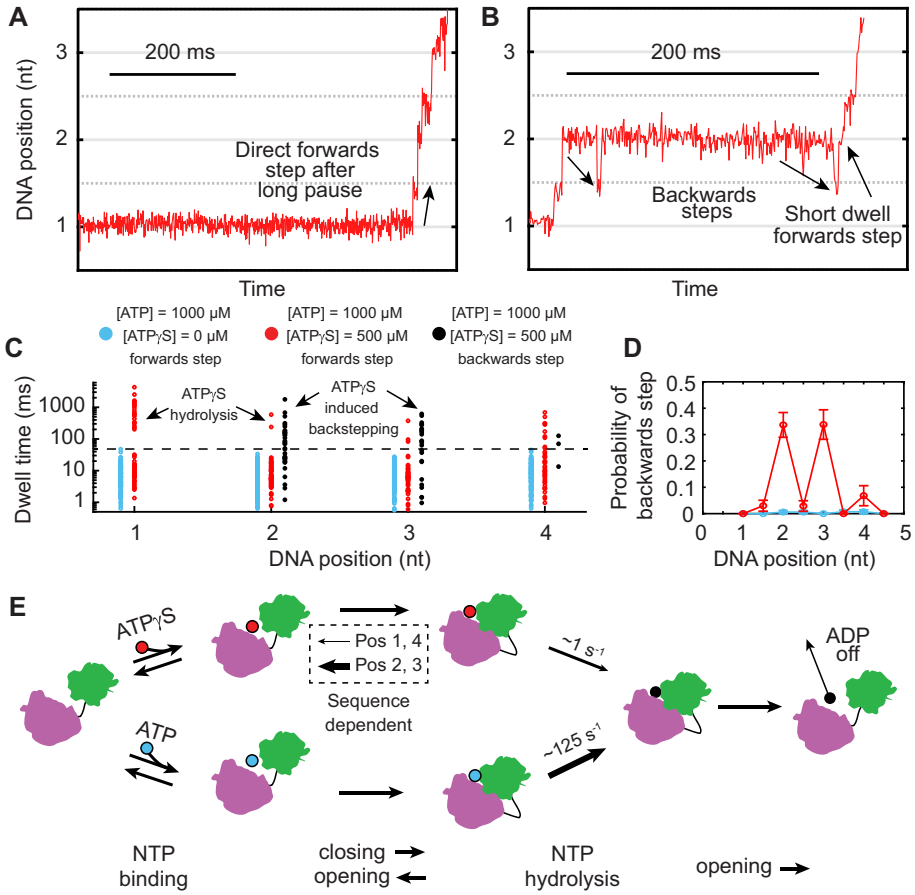

Figure 3. Sequence-dependent RecQ kinetics revealed by ATPγS binding. (**A**) Position vs. time trace demonstrating ATPγS hydrolysis by RecQ at DNA position 1. (**B**) Position versus time trace demonstrating backwards steps of RecQ induced by ATPγS at DNA position 2. (**C**) Dwell-times versus DNA position for [ATP]-independent flf steps at [ATP] = 1000 μM and [ATPγS] = 0 μM (blue), flf steps in the presence of 500 μM ATPγS (red) and blf steps in the presence of 500 μM ATPγS (black). The black dashed line is to guide the eye to the scale separation in the dwell time distributions when ATPγS was present. (**D**) Probability of backwards step versus DNA position at [ATP] = 1000 μM and [ATPγS] = 0 μM (blue) and at [ATP] = 1000 μM and [ATPγS] = 500 μM (red). (**E**) Model describing RecQ behavior in mixed ATP/ATPγS conditions. The RecA-like domains of RecQ are represented in purple and green. ATP and ATPγS compete for the binding site at the interface between the RecA-like domains. Upon NTP binding the RecA-like domains adopt a closed conformation. If ATP is bound, RecQ continues through the hydrolysis pathway. If ATPγS is bound, RecQ can either slowly hydrolyze ATPγS (positions 1, 4) or transiently open and eject ATPγS (positions 2, 3).

suggest that the underlying ssDNA sequence modifies the opening and closing rates of the RecA domains by changing the relative binding strength of the individual RecA-like domains.

These data provide insights into the dissociation pathway of RecQ from DNA. In typical experiments with saturating [ATP] and [ATPγS] = 0, the RecQ remained bound to the DNA for ∼500 ms during which it translocated ∼10 nt. In experiments with ATPγS, RecQ remained bound for much longer periods of time, but still only translocated ∼10 nt, demonstrating that there is a dissociation probability per nucleotide translocated rather than per unit time. Because most of the pause duration is spent in the [ATP]-independent state with ATPγS bound (closed conformation, Figure 2), we conclude RecQ is tightly bound to the DNA in the closed conformation with ATPγS bound. Sarlos *et al*. found that RecQ is most stable when bound to ATP or ADP + phosphate, whereas it is least stable when bound to ADP (38). Our results are in reasonable agreement with their findings: ATP binding shifts equilibrium towards the closed conformation, which we postulate is stable. Hydrolysis occurs in the closed conformation, resulting in the formation of ADP + phosphate. Similarly, ADP alone causes a shift in equilibrium from the closed to open conformation, which is the least stable DNA bound state (Discussion S4).

RecQ translocation on single-stranded DNA

We next measured RecQ translocation on ssDNA under varying assisting and opposing forces to understand how RecQ generates and responds to mechanical forces and to determine the energy landscape of RecQ motion (Figure 1B, C). For these experiments, we used a poly-T ssDNA template to minimize sequence-dependent effects (Supplementary Figure S4). Figure 4A shows several position versus time traces of RecQ translocation on ssDNA with either 37 pN assisting force or 37 pN opposing force. The dwell-times of [ATP]-dependent and [ATP]-independent states in both geometries were similar (∼8 ms), however with opposing force many more backwards steps were observed from

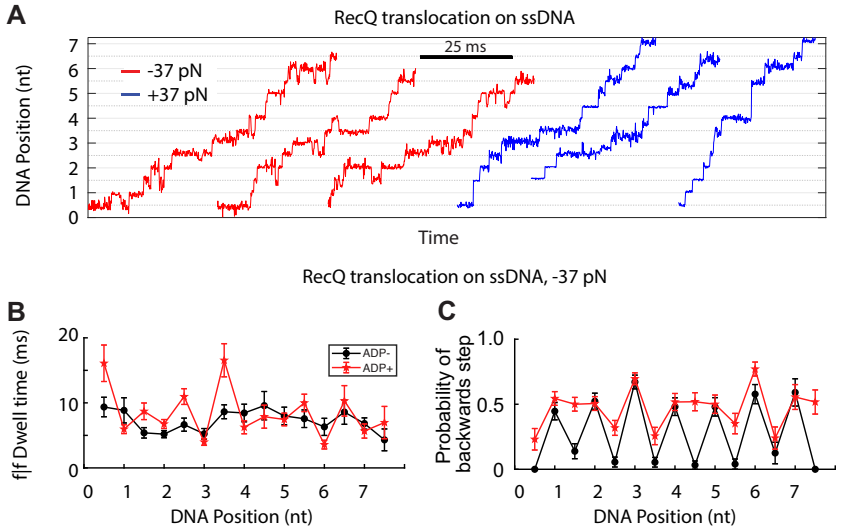

Figure 4. RecQ translocation on ssDNA. (**A**) Position versus time traces for RecQ translocation on ssDNA under an applied force of –37 pN (red) and +37 pN (blue). The time scale indicates 25 ms. On average, the translocation velocity under an opposing force is slower and backwards steps are observed much more frequently. (**B**) f|f dwell time versus DNA position for RecQ translocation on ssDNA with 37 pN opposing force in the absence of ADP (black) and with equimolar ATP and ADP (red). Errors are SEM. (**C**) Probability of a backwards step versus DNA position for RecQ translocation on ssDNA with 37 pN opposing force in the absence of ADP (black) and equimolar ATP and ADP (red). Errors are SEM.

both open and closed states, leading to a reduced average velocity of the helicase.

We then compared how the kinetics of RecQ were altered by ADP in force assisting and force-opposing geometries (Figure 4B, C, Table 1). In the force-assisting configuration, the presence of equimolar ADP and ATP resulted in longer [ATP]-dependent state dwell-times but did not increase the probability of a backwards step. In the force-opposing configuration, the presence of equimolar ATP and ADP increased the dwell-time to a lesser extent than in the force-assisting configuration, however the probability of a backwards step was significantly increased. These results suggest that ADP lowers the activation energy for a conformational change that results in backwards motion along the DNA strand. Assisting force discourages this conformational change, resulting in longer dwell times of the open conformation in the presence of ADP, whereas opposing force encourages this backwards step from open to closed.

Notably, these experiments were done in the absence of phosphate, indicating that ADP alone is sufficient to cause backwards steps from the [ATP]-dependent state. This finding suggests that phosphate unbinding may occur while RecQ is in the closed state, immediately after ATP hydrolysis during the [ATP]-independent (closed) state.

Applying transition state theory to reveal the energy landscape of RecQ translocation on ssDNA

We turned to transition state theory to understand how the RecQ responds to mechanical force (Supplementary Figures S7–S12, Supplementary Table S3). In transition state theory the coupling of kinetics to force depends on *both* the magnitude of the applied force (voltage) and the distance to the transition state along the reaction coordinate. Figure 5A, B shows two schematic energy landscapes for a hypothetical enzyme step that results in DNA motion through the pore. The reaction coordinate in this landscape is the DNA position, x, in the MspA nanopore. The distance between energy minima, x_{step}, is measured in SPRNT (Materials and Methods, Supplementary Figure S8).

In the absence of applied force, the free-energy landscapes shown in Figure 5A and B have the same activation energies ΔE_+ and ΔE_-, corresponding to transition rates k_+ and k_-, and free energy difference, ΔG_0, between the energy minima. Only the coordinate of the transition state x_t differs between the two diagrams. In the first energy landscape (Figure 5A), the transition state is located close to the first energy well ($x_t \sim 0$) and in the second energy landscape (Figure 5B) the transition state is located close to the second energy well ($x_t \sim x_{\mathrm{step}}$). Application of an assisting force F modifies each energy landscape:

$$E_F(x) = E_0(x) - F \cdot x \tag{1}$$

where x is the reaction coordinate and $E(x)$ is the energy along x. Each of these modified landscapes has the same free energy difference between the initial and final states ΔG_F and therefore the equilibrium probability of being in either energy well is unchanged. However, because the rates k_+ and k_- are determined by the activation energy, they are modified differently by the application of the mechanical force. In the first landscape (Figure 5C), k_+ is nearly unchanged because the force acts over a small distance, whereas k_- is reduced because the energy barrier to go backwards is heightened. Similarly, in the second landscape k_+ is increased due to the lowering of the activation energy, whereas k_- is unchanged (Figure 5D).

Figure 6A shows the kinetic model of RecQ. There are two mechanical transitions associated with RecQ conformational changes that perform work by moving DNA through the pore: opening and closing of the RecA-like domains with either ATP bound (k_{ST} and $k_{-\mathrm{ST}}$, closing/opening) or ADP bound (k_{SD} and $k_{-\mathrm{SD}}$, opening/closing). These are the only rate constants sensitive

Table 1. Effects of ADP on RecQ translocation

Kinetic measurement	[ATP]-independent [ADP] = 0	[ATP]-independent [ADP] = [ATP]	[ATP]-dependent [ADP] = 0	[ATP]-dependent [ADP] = [ATP]
Dwell time (ms) +37 pN	7.3 ± 0.3	7.1 ± 0.4	8.5 ± 0.4	17 ± 1
Probability of backwards step +37 pN	0.003 ± 0.002	0	0.008 ± 0.004	0.005 ± 0.005
Dwell time (ms) –37 pN	7.0 ± 0.5	6.1 ± 0.3	7.4 ± 0.5	10.1 ± 0.6
Probability of backwards step –37 pN	0.51 ± 0.02	0.53 ± 0.02	0.07 ± 0.02	0.37 ± 0.03

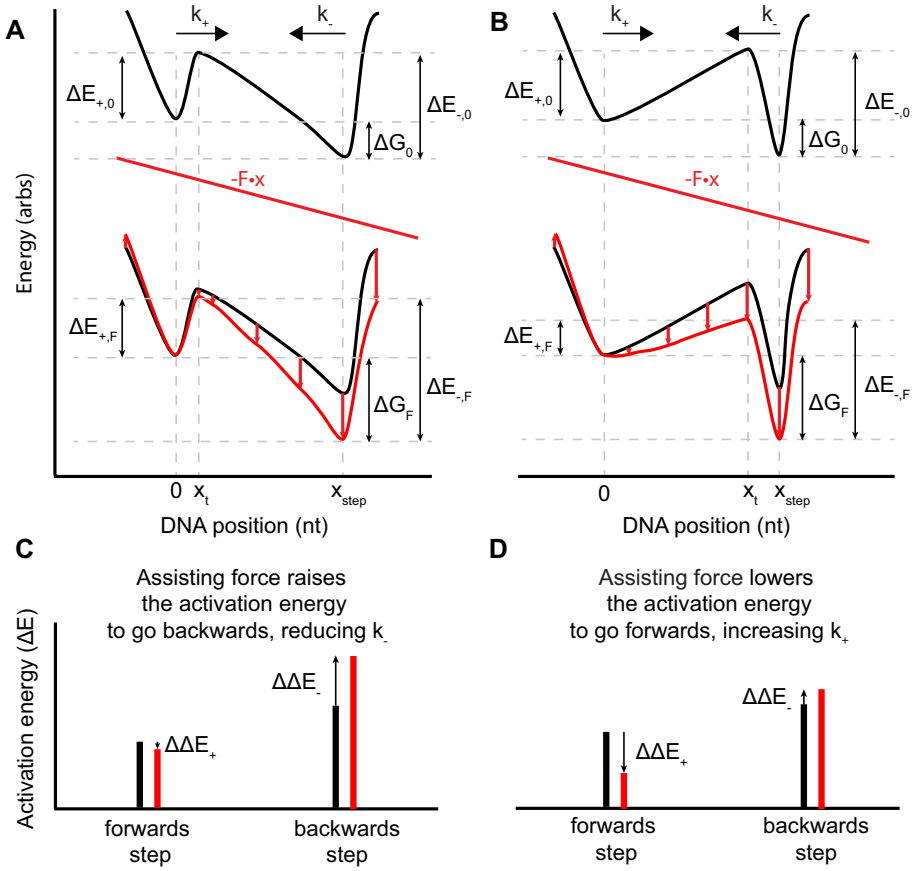

Figure 5. Effects of force in nanopore tweezers. (**A**) A schematic energy landscape for a step between two states at position $x = 0$ and $x = x_{step}$ along a reaction coordinate given by the DNA position in MspA. The step size is indicated by x_{step}. In this framework, the enzyme makes a step from $x = 0$ to $x = x_{step}$ once thermal fluctuations exceed the height of the energy barrier located at x_t. If a force is applied to the enzyme along the reaction coordinate, energy is added to the system where the amount of energy added is given by the work done on the system $-F \bullet x$, resulting in a modified energy landscape (red curve, bottom). (**B**) The same energy diagram as in (A), but the coordinate of the transition state has been changed to be closer to x_{step}. (**C**) The activation energy for the forwards and reverse rates in the absence of force (black) and in the presence of an applied force (red) for the energy landscape shown in (A). (**D**) The activation energy for the forwards and reverse rates in the absence of force (black) and in the presence of an applied force (red) for the energy landscape shown in (B). Forwards (k_+) and backwards (k_-) rates are affected differently depending on where the transition state resides relative to $x = 0$ and x_{step}.

to the applied force because they are the only kinetic steps in which RecQ performs mechanical work on the DNA. We model these rate constants as being exponentially dependent on the force (39–43), which is directly proportional to the applied voltage V:

$$k_{ST}(V) = k_{ST,0} \exp(x_{T1} \cdot \alpha_T \cdot V) \quad (2)$$

$$k_{-ST}(V) = k_{-ST,0} \exp\left((x_{T1} - x_{step1}) \cdot \alpha_T \cdot V\right). \quad (3)$$

Similar expressions apply to k_{SD} and k_{-SD}. Where x_{step1} is the physical step size for a given step, x_{T1} is the distance between the first bound state and the transition state, and α determines how the applied voltage affects the energy landscape. α can be thought of as an effective charge per nucleotide and has units of 1/(nucleotide·voltage) (Discussion S7). Combined, the quantity '$x_{T1} \cdot \alpha_T \cdot V$' or '$(x_{T1} - x_{step1}) \cdot \alpha_T \cdot V$' represents how kinetic rates respond to the applied voltage. By using our observables to de-

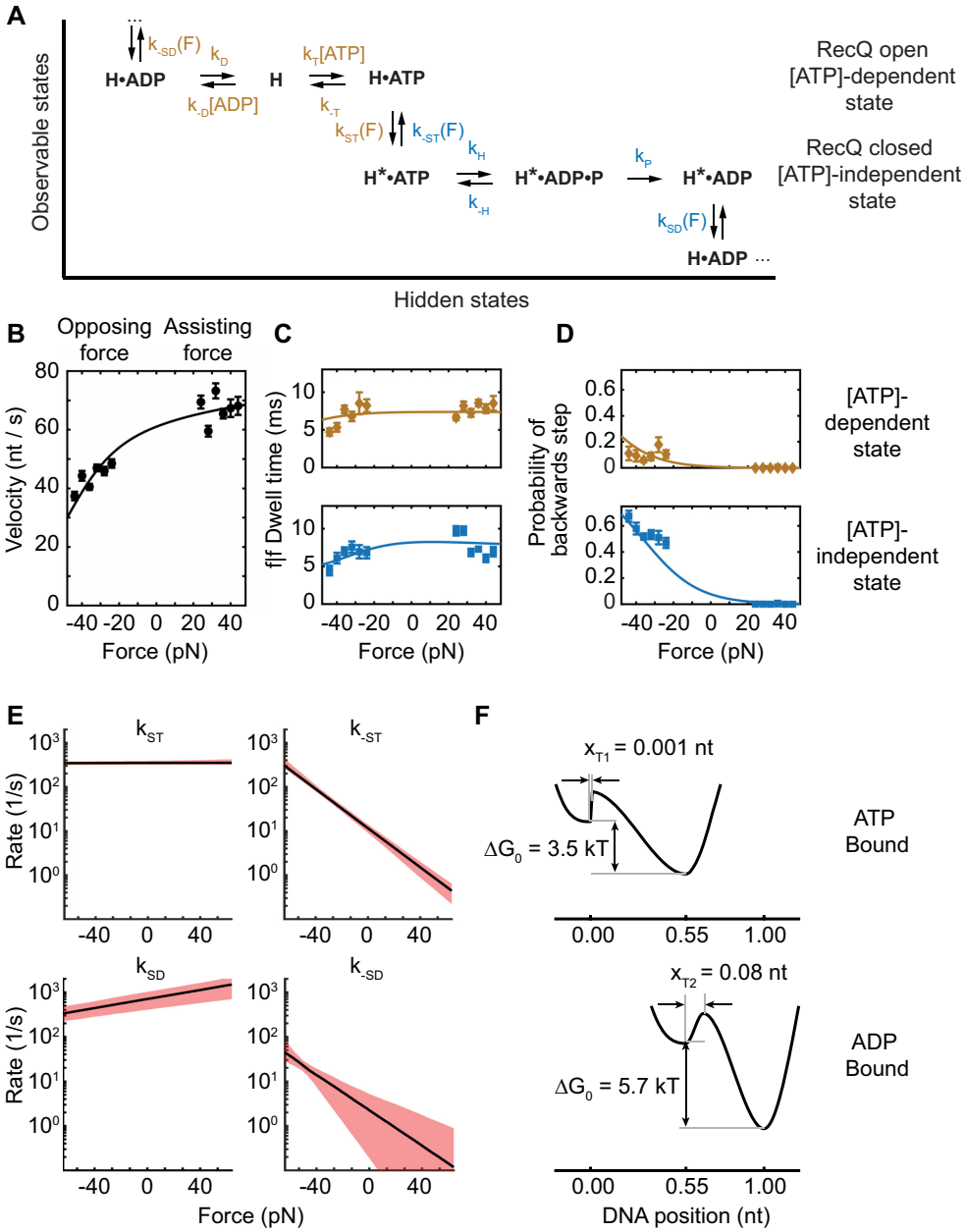

Figure 6. Force-dependent kinetics of RecQ translocation on ssDNA at saturating [ATP]. (**A**) Kinetic model of RecQ translocation on ssDNA. Rate-constants in gold affect the kinetics of the [ATP]-dependent step, rate-constants in blue affect the [ATP]-independent step. 'H' represents RecQ in the open conformation whereas 'H*' indicates RecQ in the closed conformation. (**B**) RecQ velocity versus force. (**C**) flf dwell time vs. force for the [ATP]-dependent state (gold, top) and the [ATP]-independent state (blue, bottom). (**D**) Probability of backwards step versus force for the [ATP]-dependent state (gold, top) and the [ATP]-independent state (blue, bottom). Solid lines in (B–D) are global fits to our kinetic model (Figure 6A). All errors are SEM. (**E**) Dependence of the kinetic rates shown in panel (A) on force. Forwards rates k_{ST} and k_{SD} are relatively force insensitive while backwards rates k_{-ST} and k_{-SD} are strongly force dependent. (**F**) Energy landscapes of RecQ motion on ssDNA for ATP-bound state (top) and ADP-bound state (bottom).

termine x_{T1}, x_{T2}, α_T, α_D, k_{ST}, k_{-ST}, k_{SD} and k_{-SD}, we can map key features of the energy landscape including the relative energies of the two observable states and the position of the transition state along the reaction coordinate (Discussion S5–S10, Supplementary Figure S7–S13).

We measured RecQ translocation across a range of forces from –40 pN to + 40 pN at saturating [ATP] to determine the parameters that define the energy landscape. Interestingly, different domains of the helicase are likely in contact with MspA during assisting and opposing force experiments (Figure 1B, C, (30)). However, for both experimental orientations we observe the same kinetics of [ATP]-dependent and [ATP]-independent states, and very similar step sizes, suggesting that the motion along the reaction coordinate (DNA position in MspA) is unchanged and that

we can model the kinetics of these configurations using the same equations.

The translocation velocity of RecQ remained nearly constant with assisting force but decreased with opposing force (Figure 6B). The decrease in velocity is not the result of a decrease in the forwards stepping rate, but rather due to an increase in the probability of transient backwards steps. The flf dwell-times of both [ATP]-dependent and [ATP]-independent sub-states are weakly dependent on force (Figure 6C), whereas the probability of a backwards step is nearly 0 at high assisting forces, but increases dramatically at high opposing forces, particularly in the [ATP]-independent state (Figure 6D).

By fitting these data to the model (Figure 6A), we determined the kinetic rates and voltage-coupling parameters for each step in the model (Table 2). We find that the backwards rates (k_{-ST} and k_{-SD}) are far more sensitive to applied force than the forwards rates (k_{ST} and k_{SD} Figure 6E), suggesting an asymmetric energy landscape in which the transition states for both physical steps are located much closer to the pre-translocated state than to the post-translocated state, similar to the scenario in figure 5A. From these data we constructed a free energy diagram for the physical steps of RecQ's hydrolysis cycle (Figure 6F). The transition state positions are calculated from figure 6E, where the quantity $x_{T1}\cdot\alpha_T$ is the slope in the fit for k_{ST} and $(x_{step1} - x_{T1})\cdot\alpha_T$ is the slope in the fit for k_{-ST}. We found that $x_{T1} = 0.001$ nt while $x_{T2} = 0.08$ nt (Discussion S10). We did not vary the temperature in these experiments, and therefore did not determine the activation energy, however previous work with Hel308 suggests that the activation energies can be as high as 10–20 kT (27). Energy differences between the open and closed conformations with ATP bound are determined by the equilibrium relationship at zero force:

$$\Delta G_{ATP,0} = kT \cdot \log\left(k_{ST,0}/k_{-ST,0}\right) \quad (4)$$

with an identical relationship for $k_{SD,0}$ and $k_{-SD,0}$ when ADP is bound to RecQ. While a zero-force measurement is not possible using Nanopore Tweezers, using our model we can interpolate to zero force (Figure 6B–E). We find that the $\Delta G_{ATP,0}$ is 3.5 ± 0.1 kT and $\Delta G_{ADP,0}$ is 5.7 ± 0.6 kT (Figure 6F). These results are consistent with molecular dynamics simulations of apo, ATP-bound and ADP-bound RecQ, which suggest that apo and ADP-bound RecQ are most often in the open conformation, whereas ATP-bound RecQ is most often in the closed conformation (Discussion S11, Supplementary Figure S14).

To gain further insight into how the location of the transition state affects RecQ kinetics we calculated how different transition state locations would affect RecQ's response to force. We did this by varying the location of the transition states within our model while leaving each of the rate constants unchanged. Figure 7 shows how the location of the transition state has a profound effect on how RecQ's velocity would respond to mechanical force (Discussion S12). When $x_t \sim 0$ RecQ velocity remains essentially constant across much of the force range and then drops off at high opposing forces (Figure 7A). As x_t approaches x_{step} RecQ would go faster with assisting forces but is also significantly slowed by even small opposing forces. With $x_t \sim 0$ for both physical steps, RecQ trades frequent, yet brief backward steps for the ability to maintain average velocity against opposing mechanical forces such as those that may be encountered *in vivo* including complex DNA secondary structures or proteins bound to DNA (Figure 7B, C). This tradeoff is enabled by the fact that at zero force, $k_{ST} >> k_{-ST}$ and $k_{SD} >> k_{-SD}$ such that k_{-ST} and k_{-SD} must increase in magnitude significantly before they are comparable to k_{ST} and k_{SD} and affect the average velocity.

Table 2. RecQ kinetic parameters

Parameter	Unit	Value	Calculation reference
$x_{step,1}$	nt	0.56 ± 0.02	discussion s5
$x_{step,2}$	nt	0.44 ± 0.02	discussion s5
x_{T1}	nt	< 0.001	discussion s9; eq s33
x_{T2}	nt	0.08 ± 0.04	discussion s9; eq s34
α_T	$mV^{-1}\cdot nt^{-1}$	0.025 ± 0.002	discussion s9; eq s33
α_D	$mV^{-1}\cdot nt^{-1}$	0.039 ± 0.014	discussion s9; eq s34
$\Delta G_{ATP,0}$	kT	3.5 ± 0.1	discussion s9; eq s37-s38
$\Delta G_{ADP,0}$	kT	5.7 ± 0.6	discussion s9; eq s37-s38
k_{SD}	s^{-1}	700 ± 100	discussion s7; eq s18
α_{SD}	mV^{-1}	0.0031 ± 0.0002	discussion s7; eq s18
k_{-SD}	s^{-1}	2.3 ± 1.4	discussion s7; eq s18
α_{-SD}	mV^{-1}	0.014 ± 0.006	discussion s7; eq s18
k_{ST}	s^{-1}	350 ± 10	discussion s7; eq s18
α_{ST}	mV^{-1}	$<10^{-5}$	discussion s7; eq s18
k_{-ST}	s^{-1}	11 ± 1	discussion s7; eq s18
α_{-ST}	mV^{-1}	0.014 ± 0.001	discussion s7; eq s18
k_D	s^{-1}	220 ± 10	discussion s7; eq s19
k_{-D}	$s^{-1}\cdot\mu M^{-1}$	4.3 ± 0.9	discussion s8; eq s30
k_H	s^{-1}	136 ± 7	discussion s7; eq s19
k_T	μM	100 ± 20	discussion s8; eq s28
k_{-T}	s^{-1}	>1000	discussion s8; eq s31
k_P	s^{-1}	>1000	discussion s7; eq s19

DISCUSSION

These results show how the different energy landscapes associated with different nucleotide bound states enable RecQ's processive motion and provide a rational for RecQ's ability to unwind DNA nearly as fast as it translocates along ssDNA. In the apo state (without ATP or ADP bound), RecQ is in an open conformation and no on-pathway steps occur. ATP binding alters the energy landscape, making a forward step favorable. RecQ then adopts a closed configuration that results in DNA advancing through the pore. The closed conformation enables ATP hydrolysis, again changing the energy landscape. This change disallows backwards steps, instead favoring another forward step associated with opening of the RecA-like domains. Once open, ADP release completes the hydrolysis cycle and RecQ returns to the apo state, generating a net motion of one full nucleotide along the DNA.

The mechanism we observe is consistent with structural and biochemical findings that have shown that a cycle of conformational changes coupled to ATP hydrolysis drive directed motion of SF1 and SF2 helicases along the DNA (2,44–52), however it was not previously accessible experimentally. With SPRNT, we follow both the RecA-like domain motions and DNA translocation, which enables the mechanochemical coupling between them to be determined with high spatiotemporal resolution. By determining the ef-

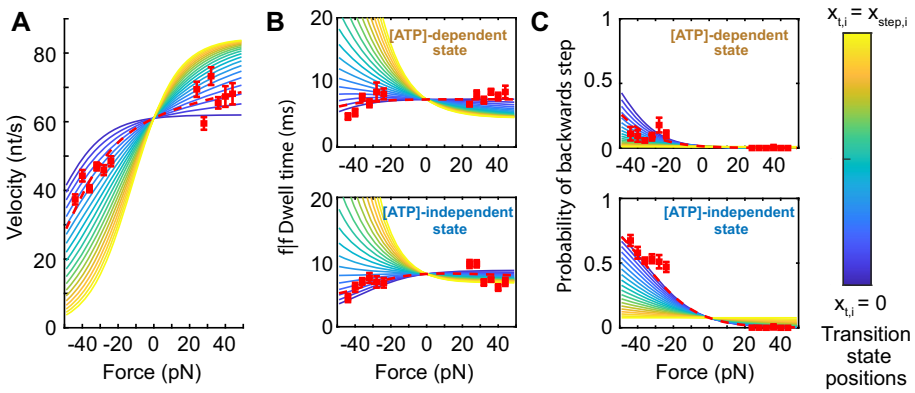

Figure 7. Simulated effects of transition state coordinate on RecQ kinetics. RecQ velocity (**A**), dwell time (**B**) and Probability of a backwards step (**C**) versus force as a function of the transition state position, assuming all other rate constants are unchanged. Blue curves correspond to both transition states located at the pre-translocated state ($x_t \sim 0$), and yellow curves to both transition states located at the post-translocated state ($x_t \sim x_{step}$). The red line is derived from our data (red squares) where $x_{t1} = 0.001$ nt and $x_{t2} = 0.08$ nt.

fects of force on the kinetics of mechanical steps, we mapped key details of RecQ's energy landscape. This revealed that RecQ generates motion through a series of chemical reactions, which alter the energy landscape, punctuated by conformational changes that move the RecA domains along the DNA in a directed manner.

The asymmetric energy landscape suggests that RecQ is optimized to maintain consistent velocity across a broad range of assisting and opposing forces (Figure 7). Opposing forces may be most relevant for RecQ, for example in stripping bound proteins from ssDNA or processing complex DNA secondary structures such as G-quadruplexes. Single-molecule studies have suggested that G-quadruplexes are highly stable, requiring forces in the 20–60 pN range to mechanically unfold (53–57). We have measured RecQ translocation against opposing forces and find that RecQ maintains a high velocity against such loads, slowing by just ∼30% despite 40 pN of opposing force. The energy landscape also explains the insensitivity of RecQ's velocity to assisting forces (Figures 6 and 7).

Helicases are characterized as 'active' or 'passive,' depending on whether they are capable of unwinding dsDNA as quickly as they translocate along ssDNA (58–60). It is thought that active helicases use part of the energy of ATP hydrolysis to destabilize the DNA duplex, whereas passive helicases rely on thermal breathing of DNA base-pairs before advancing (58). In support of this hypothesis, structural studies have identified 'wedge' structures that are thought to help pry DNA bases apart as the helicase advances (50,61–64). However some helicases including *E. coli* RecQ, maintain robust unwinding activity after deletion or mutation of this structure (65–68), suggesting other mechanisms for achieving high unwinding activity exist. An asymmetric energy landscape as was found here for RecQ may be another general mechanism through which helicases achieve high unwinding activity. Because RecQ is relatively insensitive to opposing forces, it can more easily unwind dsDNA bases without a significant decrease in translocation rate.

The core mechanism of RecQ translocation is similar to that of Hel308. This mechanism may apply generally to processive SF2 helicases. However, important mechanistic differences underlying their different physiological roles exist among these helicases and SPRNT analysis can be used to resolve these differences. For example, in Hel308 we resolved a 'futile hydrolysis' pathway in which ATP is hydrolyzed but does not produce a forwards step, which contributes significantly to Hel308 stepping kinetics in certain sequence contexts (27,29). In RecQ, we rule out this pathway as contributing to RecQ's stepping rate. Hel308 has a processivity of ∼1000 nt in SPRNT against opposing forces, whereas RecQ has a processivity of ∼10 nt in both assisting and opposing force experiments. This could be due structural differences in the way these helicases bind to DNA. Hel308 completely encircles the DNA, making contact with several DNA bases at both the sugar-phosphate backbone and the nucleobase during translocation (49), whereas RecQ binds the DNA only on one side (Figure 1D). Hel308's processivity decreases at low [ATP], suggesting that it primarily dissociates from DNA in the apo open conformation, whereas RecQ is thought to dissociate during the ADP-bound open conformation.

Single-molecule experiments provide details of the mechanical and chemical activities of enzymes. This is particularly important for understanding how small differences in enzyme structure across classes of closely related enzymes can produce different behaviors. SPRNT's high spatiotemporal resolution, in particular its ability to resolve kinetic *substates* of RecQ's ATPase cycle, enabled us to derive new details about this important class of molecular motors, beyond what was previously accessible. The SPRNT experimental and analytical framework developed here to interpret RecQ behavior can be broadly applied to obtain mechanistic insights and quantify kinetic and energetic parameters in other enzyme systems.

DATA AVAILABILITY

All raw data, analysis products and code are available in figshare (DOI: 10.6084/m9.figshare.17757185).

SUPPLEMENTARY DATA

Supplementary Data are available at NAR Online.

ACKNOWLEDGEMENTS

We thank Gabor Harami and Mihaly Kovacs for providing some of the RecQ enzyme used in this study and interesting discussions on SF2 helicases. We thank David Blum and Alan Hoofring from the Medical Arts group at the National Institutes of Health for creating the animation. We thank Christopher Thomas and Henry Brinkerhoff for helpful comments and critical reading of the manuscript.

FUNDING

National Human Genome Research Institute [R01HG005115 to J.M.C., A.H.L., S.J.A., H.C.K., J.R.H., J.W.M., J.H.G.]; National Heart, Lung, and Blood Institute, National Institutes of Health, Intramural Research Program [HL001056-14 to K.C.N., M.M., in part]. Funding for open access charge: National Human Genome Research Institute [R01HG005115].

Conflict of interest statement. J.M.C., A.H.L., J.H.G. and the University of Washington have a patent on the SPRNT technology (US patent number 10359395).

REFERENCES

1. Mackintosh,S.G. and Raney,K.D. (2006) DNA unwinding and protein displacement by superfamily 1 and superfamily 2 helicases. *Nucleic Acids Res.*, **34**, 4154–4159.
2. Singleton,M.R., Dillingham,M.S. and Wigley,D.B. (2007) Structure and mechanism of helicases and nucleic acid translocases. *Annu. Rev. Biochem.*, **76**, 23–50.
3. Fairman-Williams,M.E., Guenther,U.-P. and Jankowsky,E. (2010) SF1 and SF2 helicases: family matters. *Curr. Opin. Struct. Biol.*, **20**, 313–324.
4. Wu,C.G. and Spies,M. (2013) Overview: what are helicases?*DNA Helicases DNA Mot. Proteins.*, **767**, 1–16.
5. Beyer,D.C., Ghoneim,M.K. and Spies,M. (2013) Structure and mechanisms of SF2 DNA helicases. In: *DNA Helicases and DNA Motor Proteins*. Springer, pp. 47–73.
6. Killoran,M.P. and Keck,J.L. (2006) Sit down, relax and unwind: structural insights into RecQ helicase mechanisms. *Nucleic Acids Res.*, **34**, 4098–4105.
7. Vindigni,A. and Hickson,I.D. (2009) RecQ helicases: multiple structures for multiple functions? *HFSP J.*, **3**, 153–164.
8. Vindigni,A., Marino,F. and Gileadi,O. (2010) Probing the structural basis of RecQ helicase function. *Biophys. Chem.*, **149**, 67–77.
9. Chu,W.K. and Hickson,I.D. (2009) RecQ helicases: multifunctional genome caretakers. *Nat. Rev. Cancer*, **9**, 644.
10. Singleton,M.R. and Wigley,D.B. (2002) Modularity and specialization in superfamily 1 and 2 helicases. *J. Bacteriol.*, **184**, 1819–1826.
11. Byrd,A.K. and Raney,K.D. (2012) Superfamily 2 helicases. *Front. Biosci. Landmark Ed.*, **17**, 2070.
12. Harmon,F.G. and Kowalczykowski,S.C. (1998) RecQ helicase, in concert with RecA and SSB proteins, initiates and disrupts DNA recombination. *Genes Dev.*, **12**, 1134–1144.
13. Harmon,F.G. and Kowalczykowski,S.C. (2001) Biochemical characterization of the DNA helicase activity of the escherichia coli RecQ helicase. *J. Biol. Chem.*, **276**, 232–243.
14. Dou,S.-X., Wang,P.-Y., Xu,H.Q. and Xi,X.G. (2004) The DNA binding properties of the escherichia coli RecQ helicase. *J. Biol. Chem.*, **279**, 6354–6363.
15. Mohaghegh,P., Karow,J.K., Brosh,R.M. Jr, Bohr,V.A. and Hickson,I.D. (2001) The bloom's and werner's syndrome proteins are DNA structure-specific helicases. *Nucleic Acids Res.*, **29**, 2843–2849.
16. Bernstein,K.A., Gangloff,S. and Rothstein,R. (2010) The RecQ DNA helicases in DNA repair. *Annu. Rev. Genet.*, **44**, 393–417.
17. Voter,A.F., Qiu,Y., Tippana,R., Myong,S. and Keck,J.L. (2018) A guanine-flipping and sequestration mechanism for G-quadruplex unwinding by RecQ helicases. *Nat. Commun.*, **9**, 4201.
18. Postberg,J., Tsytlonok,M., Sparvoli,D., Rhodes,D. and Lipps,H.J. (2012) A telomerase-associated RecQ protein-like helicase resolves telomeric G-quadruplex structures during replication. *Gene*, **497**, 147–154.
19. Budhathoki,J.B., Ray,S., Urban,V., Janscak,P., Yodh,J.G. and Balci,H. (2014) RecQ-core of BLM unfolds telomeric G-quadruplex in the absence of ATP. *Nucleic Acids Res.*, **42**, 11528–11545.
20. Smestad,J.A. and Maher,L.J. (2015) Relationships between putative G-quadruplex-forming sequences, RecQ helicases, and transcription. *BMC Med. Genet.*, **16**, 91.
21. Manosas,M., Meglio,A., Spiering,M.M., Ding,F., Benkovic,S.J., Barre,F.-X., Saleh,O.A., Allemand,J.F., Bensimon,D. and Croquette,V. (2010) Magnetic tweezers for the study of DNA tracking motors. *Methods Enzymol.*, **475**, 297–320.
22. Harami,G.M., Seol,Y., In,J., Ferencziová,V., Martina,M., Gyimesi,M., Sarlós,K., Kovács,Z.J., Nagy,N.T., Sun,Y. *et al.* (2017) Shuttling along DNA and directed processing of D-loops by RecQ helicase support quality control of homologous recombination. *Proc. Natl. Acad. Sci. U.S.A.*, **114**, E466–E475.
23. Seol,Y., Strub,M.-P. and Neuman,K.C. (2016) Single molecule measurements of DNA helicase activity with magnetic tweezers and t-test based step-finding analysis. *Methods*, **105**, 119–127.
24. Seol,Y., Harami,G.M., Kovács,M. and Neuman,K.C. (2019) Homology sensing via non-linear amplification of sequence-dependent pausing by RecQ helicase. *Elife*, **8**, e45909.
25. Derrington,I.M., Craig,J.M., Stava,E., Laszlo,A.H., Ross,B.C., Brinkerhoff,H., Nova,I.C., Doering,K., Tickman,B.I., Ronaghi,M. *et al.* (2015) Subangstrom single-molecule measurements of motor proteins using a nanopore. *Nat. Biotechnol.*, **33**, 1073–1075.
26. Laszlo,A.H., Derrington,I.M. and Gundlach,J.H. (2016) MspA nanopore as a single-molecule tool: from sequencing to SPRNT. *Methods*, **105**, 75–89.
27. Craig,J.M., Laszlo,A.H., Brinkerhoff,H., Derrington,I.M., Noakes,M.T., Nova,I.C., Tickman,B.I., Doering,K., de Leeuw,N.F. and Gundlach,J.H. (2017) Revealing dynamics of helicase translocation on single-stranded DNA using high-resolution nanopore tweezers. *Proc. Natl. Acad. Sci. U.S.A.*, **114**, 11932–11937.
28. Craig,J.M., Laszlo,A.H., Nova,I.C., Brinkerhoff,H., Noakes,M.T., Baker,K.S., Bowman,J.L., Higinbotham,H.R., Mount,J.W. and Gundlach,J.H. (2019) Determining the effects of DNA sequence on hel308 helicase translocation along single-stranded DNA using nanopore tweezers. *Nucleic Acids Res.*, **47**, 2506–2513.
29. Craig,J.M., Laszlo,A.H., Nova,I.C. and Gundlach,J.H. (2021) Modelling single-molecule kinetics of helicase translocation using high-resolution nanopore tweezers (SPRNT). *Essays Biochem.*, **65**, 109–127.
30. Laszlo,A.H., Craig,J.M., Gavrilov,M., Tippana,R., Nova,I.C., Huang,J.R., Kim,H.C., Abell,S.J., deCampos-Stairiker,M., Mount,J.W. *et al.* (2022) Sequence-dependent mechanochemical coupling of helicase translocation and unwinding at single-nucleotide resolution. bioRxiv doi: https://doi.org/10.1101/2022.02.10.479955, 11 February 2022, preprint: not peer reviewed.
31. Butler,T.Z., Pavlenok,M., Derrington,I.M., Niederweis,M. and Gundlach,J.H. (2008) Single-molecule DNA detection with an engineered MspA protein nanopore. *Proc. Natl. Acad. Sci.*, **105**, 20647–20652.
32. Tsygankov,D., Lindén,M. and Fisher,M.E. (2007) Back-stepping, hidden substeps, and conditional dwell times in molecular motors. *Phys. Rev. E*, **75**, 021909.
33. Chemla,Y.R., Moffitt,J.R. and Bustamante,C. (2008) Exact solutions for kinetic models of macromolecular dynamics. *J. Phys. Chem. B*, **112**, 6025–6044.
34. Bernstein,D.A., Zittel,M.C. and Keck,J.L. (2003) High-resolution structure of the e. coli RecQ helicase catalytic core. *EMBO J.*, **22**, 4910–4921.
35. Bredenberg,J. and Nilsson,L. (2001) Modeling zinc sulfhydryl bonds in zinc fingers. *Int. J. Quantum Chem.*, **83**, 230–244.
36. Phillips,J.C., Hardy,D.J., Maia,J.D., Stone,J.E., Ribeiro,J.V., Bernardi,R.C., Buch,R., Fiorin,G., Hénin,J. and Jiang,W. (2020) Scalable molecular dynamics on CPU and GPU architectures with NAMD. *J. Chem. Phys.*, **153**, 044130.
37. Humphrey,W., Dalke,A. and Schulten,K. (1996) VMD: visual molecular dynamics. *J. Mol. Graph.*, **14**, 33–38.

38. Sarlós,K., Gyimesi,M., Kele,Z. and Kovács,M. (2015) Mechanism of RecQ helicase mechanoenzymatic coupling reveals that the DNA interactions of the ADP-bound enzyme control translocation run terminations. *Nucleic Acids Res.*, **43**, 1090–1097.
39. Wang,M.D., Schnitzer,M.J., Yin,H., Landick,R., Gelles,J. and Block,S.M. (1998) Force and velocity measured for single molecules of RNA polymerase. *Science*, **282**, 902–907.
40. Block,S.M., Asbury,C.L., Shaevitz,J.W. and Lang,M.J. (2003) Probing the kinesin reaction cycle with a 2D optical force clamp. *Proc. Natl. Acad. Sci. U.S.A.*, **100**, 2351–2356.
41. Clemen,A.E.-M., Vilfan,M., Jaud,J., Zhang,J., Bärmann,M. and Rief,M. (2005) Force-dependent stepping kinetics of myosin-V. *Biophys. J.*, **88**, 4402–4410.
42. Veigel,C., Schmitz,S., Wang,F. and Sellers,J.R. (2005) Load-dependent kinetics of myosin-V can explain its high processivity. *Nat. Cell Biol.*, **7**, 861–869.
43. Walcott,S. (2008) The load dependence of rate constants. *J. Chem. Phys.*, **128**, 06B601.
44. Velankar,S.S., Soultanas,P., Dillingham,M.S., Subramanya,H.S. and Wigley,D.B. (1999) Crystal structures of complexes of PcrA DNA helicase with a DNA substrate indicate an inchworm mechanism. *Cell*, **97**, 75–84.
45. Lee,J.Y. and Yang,W. (2006) UvrD helicase unwinds DNA one base pair at a time by a two-part power stroke. *Cell*, **127**, 1349–1360.
46. Kim,J.L., Morgenstern,K.A., Griffith,J.P., Dwyer,M.D., Thomson,J.A., Murcko,M.A., Lin,C. and Caron,P.R. (1998) Hepatitis c virus NS3 RNA helicase domain with a bound oligonucleotide: the crystal structure provides insights into the mode of unwinding. *Structure*, **6**, 89–100.
47. Korolev,S., Hsieh,J., Gauss,G.H., Lohman,T.M. and Waksman,G. (1997) Major domain swiveling revealed by the crystal structures of complexes of e. coli rep helicase bound to single-stranded DNA and ADP. *Cell*, **90**, 635–647.
48. Gu,M. and Rice,C.M. (2010) Three conformational snapshots of the hepatitis c virus NS3 helicase reveal a ratchet translocation mechanism. *Proc. Natl. Acad. Sci. U.S.A.*, **107**, 521–528.
49. Büttner,K., Nehring,S. and Hopfner,K.-P. (2007) Structural basis for DNA duplex separation by a superfamily-2 helicase. *Nat. Struct. Mol. Biol.*, **14**, 647–652.
50. Saikrishnan,K., Griffiths,S.P., Cook,N., Court,R. and Wigley,D.B. (2008) DNA binding to recd: role of the 1B domain in SF1B helicase activity. *EMBO J.*, **27**, 2222–2229.
51. Dillingham,M.S., Wigley,D.B. and Webb,M.R. (2000) Demonstration of unidirectional single-stranded DNA translocation by PcrA helicase: measurement of step size and translocation speed. *Biochemistry*, **39**, 205–212.
52. Gyimesi,M., Sarlos,K. and Kovacs,M. (2010) Processive translocation mechanism of the human bloom's syndrome helicase along single-stranded DNA. *Nucleic Acids Res.*, **38**, 4404–4414.
53. Yu,Z., Schonhoft,J.D., Dhakal,S., Bajracharya,R., Hegde,R., Basu,S. and Mao,H. (2009) ILPR G-Quadruplexes formed in seconds demonstrate high mechanical stabilities. *J. Am. Chem. Soc.*, **131**, 1876–1882.
54. Pandey,S., Li,Y., Young,M.D., Mandal,S., Lu,L., Shelley,J.T. and Mao,H. (2020) Cooperative heteroligand interaction with G-Quadruplexes shows evidence of allosteric binding. *Biochemistry*, **59**, 3438–3446.
55. Yangyuoru,P.M., Di Antonio,M., Ghimire,C., Biffi,G., Balasubramanian,S. and Mao,H. (2015) Dual binding of an antibody and a small molecule increases the stability of TERRA G-Quadruplex. *Angew. Chem. Int. Ed.*, **54**, 910–913.
56. Abraham Punnoose,J., Ma,Y., Hoque,M.E., Cui,Y., Sasaki,S., Guo,A.H., Nagasawa,K. and Mao,H. (2018) Random formation of G-Quadruplexes in the full-length human telomere overhangs leads to a kinetic folding pattern with targetable vacant G-Tracts. *Biochemistry*, **57**, 6946–6955.
57. Yang,D. and Lin,C. (eds). (2019) *G-Quadruplex Nucleic Acids: Methods and Protocols*. Springer, NY.
58. Betterton,M.D. and Jülicher,F. (2005) Opening of nucleic-acid double strands by helicases: active versus passive opening. *Phys. Rev. E Stat. Nonlin. Soft Matter Phys.*, **71**, 011904.
59. Manosas,M., Xi,X.G., Bensimon,D. and Croquette,V. (2010) Active and passive mechanisms of helicases. *Nucleic Acids Res.*, **38**, 5518–5526.
60. Yodh,J.G., Schlierf,M. and Ha,T. (2010) Insight into helicase mechanism and function revealed through single-molecule approaches. *Q. Rev. Biophys.*, **43**, 185–217.
61. Bhattacharyya,B. and Keck,J.L. (2014) Grip it and rip it: structural mechanisms of DNA helicase substrate binding and unwinding. *Protein Sci.*, **23**, 1498–1507.
62. Lucic,B., Zhang,Y., King,O., Mendoza-Maldonado,R., Berti,M., Niesen,F.H., Burgess-Brown,N.A., Pike,A.C., Cooper,C.D. and Gileadi,O. (2011) A prominent β-hairpin structure in the winged-helix domain of RECQ1 is required for DNA unwinding and oligomer formation. *Nucleic Acids Res.*, **39**, 1703–1717.
63. Singleton,M.R., Scaife,S. and Wigley,D.B. (2001) Structural analysis of DNA replication fork reversal by recG. *Cell*, **107**, 79–89.
64. Sengoku,T., Nureki,O., Nakamura,A., Kobayashi,S. and Yokoyama,S. (2006) Structural basis for RNA unwinding by the DEAD-box protein drosophila vasa. *Cell*, **125**, 287–300.
65. Pike,A.C., Shrestha,B., Popuri,V., Burgess-Brown,N., Muzzolini,L., Costantini,S., Vindigni,A. and Gileadi,O. (2009) Structure of the human RECQ1 helicase reveals a putative strand-separation pin. *Proc. Natl. Acad. Sci. U.S.A.*, **106**, 1039–1044.
66. Pike,A.C., Gomathinayagam,S., Swuec,P., Berti,M., Zhang,Y., Schnecke,C., Marino,F., Von Delft,F., Renault,L. and Costa,A. (2015) Human RECQ1 helicase-driven DNA unwinding, annealing, and branch migration: insights from DNA complex structures. *Proc. Natl. Acad. Sci. U.S.A.*, **112**, 4286–4291.
67. Swan,M.K., Legris,V., Tanner,A., Reaper,P.M., Vial,S., Bordas,R., Pollard,J.R., Charlton,P.A., Golec,J.M. and Bertrand,J.A. (2014) Structure of human bloom's syndrome helicase in complex with ADP and duplex DNA. *Acta Crystallogr. D Biol. Crystallogr.*, **70**, 1465–1475.
68. Kitano,K. (2014) Structural mechanisms of human RecQ helicases WRN and BLM. *Front. Genet.*, **5**, 366.